IEEE Access
Multidisciplinary ⋮ Rapid Review ⋮ Open Access Journal

Received March 27, 2019, accepted April 14, 2019, date of current version May 6, 2019.

Digital Object Identifier 10.1109/ACCESS.2019.2911866

Indoor Corridor and Office Propagation Measurements and Channel Models at 8, 9, 10 and 11 GHz

IURY DA SILVA BATALHA, ANDRÉA V. R. LOPES, JASMINE P. L. ARAÚJO, (Member, IEEE), BRUNO L. S. CASTRO, FABRÍCIO J. B. BARROS, GERVÁSIO PROTÁSIO DOS SANTOS CAVALCANTE, (Member, IEEE), AND EVALDO GONÇALVES PELAES, (Member, IEEE)

Laboratory of Computer and Telecommunications, Institute of Technology, Federal University of Pará, Pará 66075-110 , Brazil

Corresponding author: Iury da Silva Batalha (iurybatalha@ufpa.br)

This work was supported in part by the CNPq and in part by the INCT.

ABSTRACT Recent research into radio propagation and large-scale channel modeling shows that frequencies can be used above 6 GHz for the new generation of mobile communications (5G). This paper provides a detailed account of measurement campaigns that use directional horn antennas in co-polarization (V-V and H-H) and cross-polarization (V-H) in line-of-sight (LOS) and obstructed-line-of-sight situations between the transmitter and receptor; they were carried out in a corridor and computer laboratory located at the Federal University of Para (UFPA). The measurement data were used to adjust path loss prediction models of radio propagation, through the minimum mean square error (MMSE) method, for indoor environments in the frequencies of 8–11 GHz. The parameters for the models that were determined are as follows: path loss exponent, polarization exponent (co- and cross-polarization), effects of shadowing and path loss exponent for wall losses. Standard deviation and standard deviation point by point are included as statistical metrics. The approximations with regard to the large-scale path loss models for frequencies of 8–11 GHz show a convergence with the measured data, owing to the method employed for the optimization of the MMSE to determine the parameters of the model.

INDEX TERMS 5G, channel modeling, path loss model, co-polarization, cross-polarization, LOS, OLOS, MMSE, measurements, 8 GHz, 9 GHz, 10 GHz and 11 GHz.

I. INTRODUCTION

The limitations of bandwidth reduce the capacity of current access technologies to provide better quality in the services offered. This limitation is caused by the frequency bands used in the global telecommunications systems which are currently fourth generation (4G) and operate on a band ranging from 700 MHz to 5 GHz [1]–[3]. The high demand for future applications in the 5G system means that more capacity is required. Most available bands are crowded in the microwave range below 6 GHz; for this reason, the microwave band above 6 GHz and the mmWave band can be used by the 5G system to meet the bandwidth required for all the 5G applications [45].

As a result of the new generation of mobile communication services (5G), there are several ongoing surveys that seek to meet the required recommendations. A key feature is channel modeling at frequencies above 6 GHz and one of the bands that received attention is the millimeter wave band [4]–[7].

The associate editor coordinating the review of this manuscript and approving it for publication was Ke Guan.

The bands have similar propagation characteristics and include the Super High Frequency (3 to 30 GHz range) with a centimeter wavelength ranging from 10 cm to 1 cm and Extremely High Frequency (30 to 300 GHz range) with a millimeter wavelength in the range of 1 at 100 mm, known as millimeter waveband [5], [6].

In investigating high frequencies and 5G, there have been a number of important research studies that have been carried out measurement and modeling campaigns in the range of 0.8 GHz to 93 GHz frequencies [4], [7]. Some organizations have also developed path loss models for millimeter waves (mmWave) [8], [8], [10], as well as 3gpp, which entailed channel studies and modeling at frequencies above 6 GHz [8]. In the FCC document [46] indicate some frequency bands for the 5G, and 10GHZ (10.125-10.225 GHz and 10.475-10.575 GHz) is presented as a potential band.

Other research studies have examined bands ranging from 10 GHz to 25 GHz and 40 GHz to 55 GHz both for indoor and outdoor environments. As shown in the report by METIS [7], which published the probable, bands needed for the 5G within these frequencies, that of 10 GHz appears to be a promising

band. Thus, this study is concerned with examining the measurements and channel modeling in the range of 8 GHz to 11 GHz frequencies for indoor environments.

As expected in [42] fifth generation (5G) mobile communication systems will be in use by 2020. The purpose of 5G systems is to provide connectivity anywhere, anytime for anyone and anything. Several new technologies are being investigated for 5G systems and one of them is the communications system using millimeter waves (mmWave). In view of the fact that channel models are indispensable for system design and performance evaluation, accurate and efficient channel models covering various technologies and 5G scenarios are urgently needed.

The indoor environment has unique features owing to the construction materials used, the number of people moving about inside, the different arrangements of the mobile devices, and interference in the systems, among other factors. Indoor environments confine the waves within the environment and have more reflective components that lead to multiple pathways, the cross sections of walls and other types of obstacles, scattering, diffraction and shadowing effects. [11].

Propagation models are of crucial importance because through them a wireless network can be planned to optimize the positions of the transmitting antennas and form a limited strategy for providing a new access technology that employs the frequencies being studied [12]. Previously, the most widely used loss models relied on linear regression (minimum mean square error - MMSE) to reduce the errors between the collected and simulated data through classical models, models such as Okumura-Hata [13], COST 231 path loss model [14] and others [15]–[17] by means of this technique. The same approach will be adopted in this study to define the parameters of the models although there are other means of modeling channels through numerical simulations and computational intelligence techniques.

One of the studies that is widespread in the research area of radio propagation modeling is ray tracing [33], [34], [38]. This technique is used to describe various bands and indoor and outdoor environments. Barros *et al.* [34] employs the Polyhedral Beam Trace (PBT) technique to model the propagation by means of the features of an indoor environment. In [36], Motorola used the PBT technique for 18GHz in 1990. In [37], the University of Bristol and Virginia Tech showed the feasibility of using ray tracing in indoor small cells.

Among the works based on measurements for frequencies above 6GHz, we can mention Deng et al., which presents diffraction models, analysis, and signal strength around objects such as corners, pillars and irregular objects at 10, 20 and 26 GHz. The diffraction measurements were performed indoors and outdoors using a channel sounding (CW) with three pairs of identical horn-type directional antennas on the transmitter and receiver [39].

The [43] made millimeter wave measurements (mmWave) in an indoor environment. In this paper, propagation characteristics in three different bands above 6 GHz (19, 28 and 38 GHz) are investigated in an indoor corridor environment for both line of sight (LOS) and non-LOS (NLOS) scenarios. Five different path loss models are studied for this environment: The Close-in (CI) model, floating interception (FI) model, frequency attenuation (FA) model, alpha-beta-gamma (ABG) model and close-in free space with frequency weighting (CIF) model. Important statistical properties, such as power delay profile (PDP), root mean square (RMS) delay interval and azimuth angle scattering are obtained and compared for the different bands. With regard to the path loss model, the results showed that the path loss exponent (PLE) is smaller than the PLE in the free space for the LOS scenario. Only the directed path is added in some spatial locations. In the case of the NLOS scenario, the angle of arrival (AOA) is extensively investigated, and the results indicated that the propagation of the channel to 5G using directional antenna should be used in the beamforming technique to receive the signal and collect all the components of multiple paths from different angles.

In article [44], there is an investigation of large-scale path loss statistics and time-scattering parameters based on ultra-wide band measurements using a directional horn antenna on the transmitter (Tx) and omnidirectional antenna on the receiver (Rx). The measurement was made in a line of sight of the dining room (LOS), which represents a typical indoor for communication in the building. Large-scale directional and omni-directional single-path and multi-parameter path loss models are evaluated in 28 GHz and 38 GHz bands based on the data acquired. The results show that the large-scale path loss models designed in this work are less complex, and even more physically based than those used in 3GPP, which involve additional parameters, but provide less accurate results. Time dispersion statistics for mmWave systems using directional antennas and a configuration of omni-omni antennas in Tx and Rx respectively, are displayed for co-polarization scenarios. We show that the delay spread can be reduced when the Tx and Rx antennas are pointed towards each other, which results in the greatest received power.

In [45] the carrier frequency is 11GHz and measurements are made with antennas with cross polarization and vertical and horizontal polarization. The PLE data for NLoS are from 2 to 3 dB and for LoS are from 0.36 to 1.5 dB. The path gain factors for vertical and horizontal media for cross-polarization were of 12.8 dB for vertical polarization and are thus similar; they only differ in NLoS situations for horizontally-polarized corridors.

Other researchers have carried out channel modeling for several frequencies. In [18] it presents radio channel characteristics in the carrier frequency of 11.2 and 14.6 GHz, with 1 GHz bandwidth in environments characterized as corridor, laboratory, offices and a conference room within a building in Beijing, China. The authors investigated the characteristics of large and small-scale fading based on realistic measurements. The characteristics of delay propagation and correlation are also discussed.

Several channel measurements were performed on the mmWave bands, e.g., bands of 6, 10, 11, 15, 18, 19, 26, 28,

32 and 38GHz in [1]; the propagation characteristics of mm-waves were investigated in a corridor with direct sight (LoS) with omni antenna in the Tx and directional antenna in the Rx with VV and VH polarization. Then, they propose the model of path loss with frequency dependence. They determined the XPD and PLE ranging from 0.1 to 1.4 dB for the frequencies.

In [19], measurements are carried out with models on a large scale in a corridor for frequencies of 14 and 22 GHz in line-of-sight (LOS) and non-line-of-sight (NLOS) conditions. A large-scale dual-slope model is designed based on the measurements needed to characterize the channel. Its validation is demonstrated through the close-in free space reference model and its parameters are defined by MMSE. Another approach involves a model based on measurements that make use of a waveguide.

The use of millimeter waves is being addressed in the current state-of-the-art and in [20] there are several large-scale measurements that rely on high gain antenna guides for frequencies of 28 GHz an 73 GHz. A model was also examined that simulates an omnidirectional antenna; this was used with the high gain antenna guides that rotate 360° in the TX and RX. The measurements were carried out in office facilities with line-of-sight (LOS) and non-line-of-sight (NLOS), by means of co-polarization (V-V) and cross-polarization (V-H). In the case of large-scale models, several models were used such as: CI, CIX, CIF, CIFX, FI, ABG and ABGX, where the path loss exponent (n) was defined through the minimum mean square error (MMSE). The random variable of the model had a zero-mean and standard deviation determined for the measured data; the random variable is given in dB. The results obtained by the authors show that the models have a high degree of accuracy when compared with the measured data.

As seen, particularly in the studies of [19] and [20], indoor measurements in bands above 6 GHz, are currently being developed owing to the need to characterize channels that have not been previously explored. The technical studies published by METIS defined 10 GHz as priority bands for the new generation of mobile technology (5G) [41]. Hence, in this study we intend to carry out a measurements campaign and channel modeling by means of path loss models. There will also be a statistical survey of the channel features for frequencies of 8 GHz, 9 GHz, 10 GHz and 11 GHz (SHF) for indoor environment, in situations such as line-of-sight (LOS) and non-line-of-sight (NLOS), by employing horn antennas, co- and cross-polarization and loss caused by obstacles (walls).

In this paper, the following systems have employed the path-loss model for single-frequency: close-in (CI) and Floating Intercept (FI), and multi-frequency models: alpha beta and gamma (ABG) and close-in frequency (CIF). The models take account of the attenuation due to the multipath and the propagation effect in indoor corridors and classrooms, as well as the polarization of the antennas, which has attracted a good deal of attention in the literature. Corridors are regarded as dielectric waveguides with transverse dimensions that are much larger than the wavelength and thus, several propagation mechanisms are involved in the process. In contrast, the classroom has a smaller transverse length and has greater width in relation to the corridor leading to a different behavior compared with it was measured in the corridor. We discuss very important propagation features in typical models of path loss in indoor environments: depolarization effects, loss of penetration through different types of walls and analysis of standard deviation in the mean or expected value and point-by-point. We conducted measurement campaigns, particularly in the 8 GHz, 9 GHz, 10 GHz and 11 GHz frequency bands and employed the single-frequency close-in (CI), Floating-intercept (IF), and multi-frequency alpha, beta and gamma and CIF models. The model parameters were determined through a linear regression of the experimental data (MMSE).

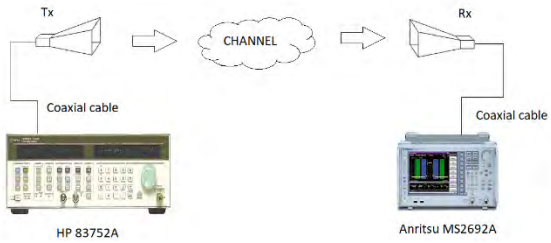

FIGURE 1. Measurement configuration for a channel survey.

The contributions of this paper are the following: (i) large-scale modeling for frequencies 8, 9, 10 and 11 GHz using co-polarized and cross-polarized antennas; (ii) study of frequency dependence between central frequencies 8, 9, 10 and 11 GHz, (iii) Analysis of the standard deviation point to point for antenna polarizations, and (iv) loss by type of obstruction (OLOS) using antennas co-polarized in the studied frequencies.

II. MEASUREMENT CAMPAIGN

A methodology for measurement is outlined in this section together with the environments and devices used for the measurement campaign and channel sounder.

A. MEASUREMENT EQUIPMENT

The measurement campaign used a HEWLETT PACKARD 83752[a]signal generator as the transmitting source and was able to transmit CW signals from 1 to 20 GHz. The ANRITSU MS2692A signal analyzer was used for the (Rx) receptor with a frequency range of 50 Hz to 26.5 GHz. Guided horn antennas were used in the experiment with a gain of 15 dBi, (29,3°/29° elevation/azimuth HPBW) for frequencies of 8 GHz, 9 GHz, 10 GHz and 11 GHz. V-V and H-H co-polarization were used for the guided horn antennas. The electric power supplied to the antenna was 15 dBm for cross-polarization measurements. Fig. 1 shows the measurement scheme with the devices and Table 1 shows the specific features of the measurement system.

TABLE 1. Channel sounder system specification for the 8, 9, 10 and 11 GHz indoor measurement campaign.

Parameter	Configuration
Center frequencies	8, 9, 10 and 11 GHz
Transmission signal	Continuous waves
Tx/Rx antenna	Horn
Tx output power	VV/HH - 0 dBm VH – 15 dBm
Tx/Rx gain	15 dBi
Tx/Rx elevation	29.3°
Tx/Rx azimuth	29°
Tx/Rx height	1.5 m
Polarization Tx	Vertical
Polarization Rx	Vertical/Horizontal

FIGURE 2. Environment For The First, Second And Fifth Measurement Campaigns (In The Corridor).

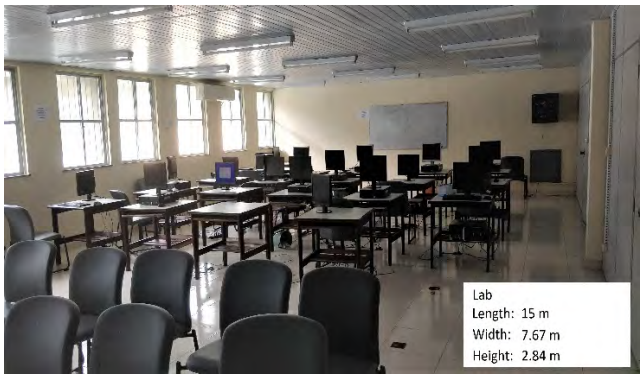

FIGURE 3. Environment For The Third, Fourth And Fifth Measurement Campaigns (In The Computer Laboratories).

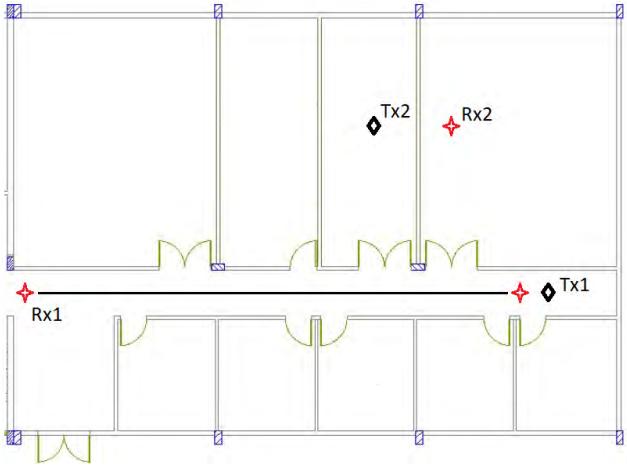

FIGURE 4. Measurement Scheme For The Corridor With LOS (Tx1 - Rx1) And The OLOS Total (Tx2 – Rx2).

B. SCENARIO AND MEASUREMENT CAMPAIGN

The measurement campaigns were carried out inside the Federal University of Pará (UFPa), in the annex to the electrical engineering laboratory and took place in the corridor and computer science laboratory. The indoor environment restricted the signaling system and led to several physical phenomena influencing the received signal. The corridor has brick walls, a cement floor with square tile flooring, wooden doors, iron grilles and a fire extinguisher (Fig. 2). The laboratory has a brick wall with glass windows and grilles (on the left side), and a completely sealed brick wall (at the front of the room), a wooden wall with a glass window and a wooden door (on the right), and another wooden wall that is completely closed off (at the back), Fig. 3.

The transmission (Tx) and reception (Rx) antennas for all the measurements was installed at a height of 1.5 m from the floor (in a typical indoor hotspot). For each Tx-Rx antenna combination the elevation defining in 0°, the azimuth varies according to the position of the receiver in the grid to obtain the maximum directivity.

During the measurement campaign, 10 measures were carried out for each meter. A grid of 25 measurement points in space was defined with a spacing of 15 cm, which is greater than the wavelength of the studied frequencies, and makes a total of 25 points for each meter. In all cases, the Tx and Rx antennas were directed. Each measuring meter is composed of a grid of 25 points, each point contains 10,001 samples of received power ($25 \times 10,001 = 250,025$) each meter were measured 10 times, totaling 2,500,250 raw data per point. Thus, for each meter traveled, there were 10 average per meter traveled. For the analysis of the figures, the spatial and temporal mean average by measured points was taken for the analysis of the statistics to determine the behavior of the data measured for the definition of the PLE.

The first measurement campaign was carried out in the corridor (Fig. 4). The transmitter (Tx) was fixed at a distance of two meters from the back wall and in the center of the corridor using a guide horn antenna with a gain of 15 dBi, co-polarization (V) and a transmission power (Pt) in dB. The receptor antenna (Rx) that had a guide horn with a gain of 15 dBi and vertical polarization (V) were positioned in the middle of the corridor where they collected 10 times data per meter. The procedure was repeated 10 times (10×25) and resulted in 250 power data in average (Pr) per measured point for the measurements in the co-polarization (V-V) corridor.

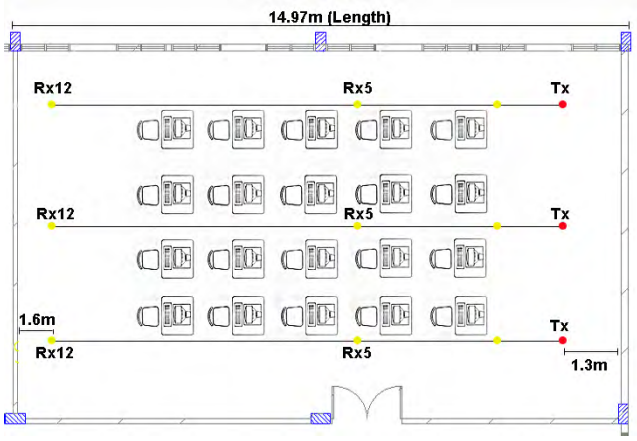

FIGURE 5. Measurement Scheme For The Laboratory In LOS.

The second measurement campaign was also carried out in the corridor and employed the same methodology as in the first campaign. However, For cross-polarization measurements, the electric power supplied to the antenna was 15 dBm. The amount of data collected was the same as for the first campaign.

The third campaign was carried out in the laboratory (Fig. 5), and the central radial point was used for all the frequencies together with the configurations of the co-polarization V-V and H-H antennas. There were three arrangements for all the frequencies - one for the transmitter (Tx), at the center and two at the extreme ends of the room that was used. A guide horn antenna with a gain of 15 dBi, co-polarization (V) and transmission power (Pt) of 0 dBm and the receptor antennas, were positioned in the same direction as the transmitters. The scenario has 12 measurement points and the procedure was repeated 10 times (10×25) resulting in more than 250 received power (Pr) per measured point.

The fourth campaign was carried out in the laboratory where the same methodology was employed with only the polarization (H-H) being altered. The same amount of measurement data was collected as before.

The fifth campaign involved measuring penetration loss through walls or other obstacles without a direct line of sight and where there was a complete obstruction. In this situation, guide horn antennas were used and co-polarization (V-V) with a gain of 15 dBi and transmission power of 0 dBm. The reason for this measurement is given by the refraction undergone in the signal which influences the propagation loss.

These losses vary in accordance with the length of the wave and the material that is crossed; in other words, the wave passes through the air, experiences refraction when it strikes an obstacle and refracts again when it returns to the air.

Three materials were used in the experiment: glass, wood and bricks. The transmitter (Tx) and receptor (Rx) antennas were fitted at a distance of 1 m from the obstacle, Fig. 4 (Tx2 and Rx2). The environments where the data were collected are the same as for the previous campaigns.

The measurement campaigns in the corridor for co- and cross-polarization (V-V and V-H respectively), only used one transmitter (Tx), with the antenna at a height of 1.5m from the floor and azimuth of 0°; the Rx was also at a height of 1.5 m from the floor and azimuth of 0°. The distance between the Tx and the Rx varied between 1 m and 15 m with 1 m steps. The measurement campaigns in the laboratory with co-polarization (V-V and H-H), 3 Tx positioned points, in the middle and corners of the room and Tx and Rx were installed at 1.5m above the floor with azimuth and an elevation at 0°. The Rx receptors were positioned in an identical way for the three radials and the directional antenna was 1.5 m above the floor with an elevation and azimuth of 0°. The distance between Tx and Rx was set at 1 m to 12 m with steps of 1 m. Only the central radial was used to analyze the measured data together with the models, owing to the fact that they were equidistant from the side walls.

The measurements for the total OLOS total were carried out in two environments. The Tx and Rx antennas were 1.5 m above the floor with an elevation and azimuth of 0°, and both were installed 1 m away from the obstacle.

The corridor and laboratory have features that influence the propagation loss within these environments. The width of the corridor is less when there are brick walls and there is a thin concrete floor as well as metal grilles and wooden doors. The laboratory is wider, has walls built of both bricks and wood and has several metal chairs, wooden tables and desktops.

Signal propagation in LOS and OLOS conditions was employed for the channel modeling and defined the PLE parameter for frequencies of 8, 9, 10 and 11 GHz, by means of the co- and cross-polarization V-V/H-H and V-H antennas respectively. The model used for the approximations is close-in free space and its extensions; MMSE is employed to reduce the standard deviation and define the parameters of the model: PLE (V-V and H-H), XPD, random variable and loss for obstacles.

III. LARGE-SCALE PATH LOSS MODELS

Large scale path loss models predict the loss from the distance between a transmitter and receptor. These models are important for wireless telecommunications systems [12]. Indoor environments exert a strong influence on electromagnetic waves such as multi-path, reflection, diffraction, penetration and shadowing effects, by affecting the power received. [21].

The large-scale loss models based on measurements provide realistic propagation features in a wireless channel [4], [19], [20], [6], [22], [23] and [24]. Most of the path loss models assume the loss can be estimated through the distance travelled on a logarithmic scale.

A. SINGLE-FREQUENCY PATH LOSS MODELS

The close-in free space reference (CI) path loss model seen in Equation (1) and given in dB, is established by a single parameter of model n, known as the path loss exponent (PLE). The CI model can be used for several frequencies with a high degree of precision for both indoor and

TABLE 2. Channel Sounding System Specifications for the 8, 9, 10 and 11 GHz Indoor Measurement Campaign.

Envir	Freq.	FSPL/β				PLE/α						γ/b		σ (dB)				XPD (dB)
		CI	FI	CIF	ABG	CI	FI	CI HH	CIX	CIF	ABG	CIF	ABG	CI	FI	CIF	ABG	
Corridor	8 GHz	50.62	50.68	50.62	49.11	2.04	2.0	-	0.65	2.07	1.8	-0.95	0.47	1.89	1.8	2.22	2	19.3
	9 GHz	51.61	53.59	51.61		2.16	1.9	-	1.59					2.58	2.5	3.57	3.55	28.7
	10 GHz	52.44	55.94	52.44		1.93	1.55	-	0.08					2.41	2.0	2.4	2.2	21.3
	11 GHz	53.35	55.62	53.35		1.73	1.44	-	0.52					2.19	1.9	2.18	2.29	14.3
Laboratory	8 GHz	50.62	50.68	50.62	29.3	2.15	2.13	2.56	-	2.18	2.1	0.1	2.39	1.18	1.1	1.17	1.17	-
	9 GHz	51.61	53.59	51.61		2.17	2.09	1.79	-					1.51	1.5	1.51	1.49	-
	10 GHz	52.44	55.94	52.44		2.07	1.98	1.81	-					0.81	0.7	1.02	0.85	-
	11 GHz	53.35	55.62	53.35		2.28	2.19	1.73	-					1.36	1.3	1.34	1.37	-

outdoor environments. Two parameters are used for indoor environments to achieve a greater precision, PLE and the random variable [6].

$$PL^{CI}(f,d)[dB] = FSPL(f,d_0) + 10n\log_{10}(\frac{d}{d_0}) + X_\sigma^{CI}$$
$$Where: FSPL(f,d_0) = 10\log_{10}(\frac{4\pi d_0}{\lambda})^2 \quad (1)$$

where X_σ^{CI} is a Gaussian random variable with zero average and standard deviation in dB [20], [25]. The CI model uses a physical base for the reference distance d_0. The path loss model uses linear regression by means of MMSE, and thus reduces the error and standard deviation. The reference distance of 1m was used in this study for the adjusted models. The CI model can be used to estimate the path in co- and cross-polarization measurements.

The CI model has an extension for loss to the cross-polarization antennas. In cross-polarization (2), a loss factor is added to the model which is called *cross-polarization discrimination* (XPD); this parameter is defined through MMSE [20] and [26]- [30].

$$PL^{CIX}(d)[dB] = FSPL + 10nlog_{10}(d) + X_\sigma^{CIX} + XPD \quad (2)$$

The parameter for attenuation and cross-polarization discrimination (XPD) is similar to the loss per floor or loss per wall [31], and the PLE of the co-polarization is used to define the best adjustment for the XPD. The XPD is employed to obtain the best value of the MMSE and reduce the error with regard to the cross-polarization measured data (by reducing the standard deviation). As seen in (2), the CIX model employs an ideal attenuation factor (XPD) and the $n_{(V-V)}$ (PLE CI), as in [20]. However, $n_{(V-V)}$ does not provide the best representation of data with V-H cross-polarized antennas; nor does it show different values from those found for the V-V co-polarized antennas, (as shown in Table 2). Thus, the PLE will be used for the CIX path loss model and for these types of cross polarization, as defined by $n_{(V-H)}$. The model seen in (2) describes the variations in the large-scale signal strength regarding the distance between the Tx and Rx using V-H cross-polarized antennas.

Another extension for the CI model is the use of H-H co-polarized antennas and in this case, the PLE is determined for this polarization (3). This parameter is similar to the PLE_{hh}, and is defined by means of the MMSE.

$$PL^{CIH}(d)[dB] = FSPL + 10nlog_{10}(d) + X_\sigma^{CIH} \quad (3)$$

where the n_{H-H} represents the path loss exponent for H-H co-polarization antennas, e X_σ^{CIHH} is a Gaussian random variable with zero average and standard deviation in dB.

Another extension planned for the CI model is for loss through different types of obstacles. An attenuation parameter was added to address the problem of obstruction - the *obstruction path loss exponent* (OPLE) - and the number of obstructions in the path of the same type (4).

$$PL^{CI} = FSPL + 10nlog_{10}(d) + X_\sigma^{CI} + \sum_{i=1}^{k} OPLE_I nw_I \quad (4)$$

where $OPLE_i$ is the path loss for the obstacle type and nw_i corresponds to the number of obstacles of the same type.

This parameter is based on the COST-231Motley-Keenan model [31]. The approach adopted to define the loss caused by the wall is to measure the received power for the same distance (3 meters), with or without obstructions [40], as defined by Equation 5.

$$OPLE = L_{meas}^{LOS}(3m) - L_{meas}^{NLOS}(3m) \quad (5)$$

where L^{LOS} is loss measured without the wall and L^{NLOS} loss with obstruction and $OPLE$ is the loss for the type of wall. The propagation models set out in this section will be analyzed in the section that follows.

The Floating-intercept (FI) path loss model is used in the WINNER II and 3GPP standards [116], [117] (6). This model

requires two parameters and does not include a physically-based anchor attached to the transmitted power.

$$PL^{FI}(d)\,[dB] = \beta + 10\alpha log_{10}(d) + X_{\sigma}^{FI} \quad (6)$$

where β is the Floating-intercept in dB (different from a FSPL reference), and α is the slope of the line (different from a PLE), also with a zero mean Gaussian (in dB) shadow fading random variable X_{σ}^{FI} which describes large-scale signal fluctuations about the mean path loss over distance.

B. MULTI-FREQUENCY PATH LOSS MODELS

The Alpha-beta-gamma path loss model (ABG) depends on distance and frequency to describe loss for several frequencies.

$$PL^{ABG} = 10\alpha log_{10}(d) + \beta + 10\gamma log_{10}(f) + X_{\sigma}^{ABG} \quad (7)$$

where α and γ are path loss parameters dependent on distance and frequency respectively. β is an optimization parameter without physical meaning. f is the frequency in GHz and X_{σ}^{ABG} is a Gaussian random variable that represents the shadowing in large-scale signal fluctuations over the mean of the path loss through distance. The ABG model is an extension of the multi-frequency FI model. The parameters α, β and γ are determined simultaneously via MMSE. The ABG parameter α is similar to the close-in PLE, just as the ABG β is similar to the close-in FSPL

A new two-parameter simple multi-frequency model can be included as an extension of the CI model. The frequency-dependent trajectory loss model (CIF) is a multifrequency model that employs the same physically motivated FSPL anchor 1 m as the CI model. The equation of the CIF model is expressed in (8):

$$PL^{CIF} = FSPL + 10n\left(1 + b\left(f - f_0/f_0\right)\right) log_{10}(d) \quad (8)$$

where n denotes the distance dependence of the trajectory loss, b is an intuitive model adjustment parameter that represents the slope of the linear frequency of path loss, f_0 is a fixed reference frequency that serves as the equilibrium point or center of the linear frequency dependence of the PLE and is based on the weighted average of all frequencies represented by the model $f_0 = \sum_{k=1}^{K} f_k N_k / \sum_{k=1}^{K} N_k$, where N_K is number of measures for each frequency and f_k is the multiplier for the corresponding frequency and X_{σ}^{CIF} is the mean Gaussian random variable zero (in dB) which describes the fluctuations of loss with distance.

IV. AN ANALISIS OF LARGE-SCALE PATH LOSS MODELS

Measurement campaigns were carried out in 8, 9, 10 and 11 GHz so that the path loss models could be used in indoor environments. The analysis and approximations for calculating signal loss were carried out in LOS and OLOS with obstruction situations. The path loss close-in distance model was used, together with the CIX in which the loss parameter was added for cross-polarization antennas. Two different environments were analyzed for four frequencies, 8, 9, 10, and 11 GHz. In the first case, the analysis was conducted in V-V co-polarization and V-H cross-polarization, and in the second case, 8, 9, 10 and 11 GHz respectively for the V-V and H-H co-polarization. There were Rx antennas for the first environment (the corridor) and for V-V, fifteen (15), fifteen (15), fourteen (14) and ten (10) for 8, 9, 10 and 11 GHz respectively. In the case of V-H antennas, there were fifteen (15) Rx, nine (9) Rx, eight (8) Rx and eight (8) Rx for the frequencies of the second environment (the lab). These were the measurements included with V-V and H-H polarization for conditions that had three (3) Tx and thirty-six (36) for the analysis of the models. The central radial point was used for analyzing the performance of the measured data, because it showed the average pattern of the three radials. The use of three radials with a) their respective PLEs b) the close-in distance path-loss model and c) its extensions are employed with the addition of a XPD cross polarization parameter, that is combined with H-H, loss for obstacles, PLE and shading effects. The performance of the models with values of PLE and standard deviation (σ), can be found in Table 2. The loss values for the obstacle path-loss exponent (OPLE) can be found in Table 3.

TABLE 3. Loss per wall for the 8, 9, 10 e 11 GHz indoor measurement campaign.

Frequency	Masonry	Wood	Glass
8 GHz	6 (dB)	0 (dB)	0 (dB)
9 GHz	8 (dB)	0 (dB)	0 (dB)
10 GHz	10 (dB)	1 (dB)	0 (dB)
11 GHz	13 (dB)	1 (dB)	0 (dB)

A. THE ANALYSIS CONDUCTED IN THE CORRIDOR

Figures 6, 7, 8 and 9 show the analysis of the measured data in the corridor together with the close-in free space reference model, FI and 3GPP for frequencies of 8, 9, 10 and 11 GHz in a logarithmic scale and in LOS conditions with directional horn antennas for V-V co-polarization, In order to compare the accuracy of the proposed model, a comparison was with the 3GPP model, calculating the standard deviation in relation to the measured data. The values determined for the corridor with the CI model were: 1.89, 2.58, 2.41 and 2.19; for the FI model the values were: 1.88, 2.51, 2.03 and 1.99; for the 3GPP model the deviation values were: 2.10, 2.59, 2.12 and 2.19 for the frequencies 8, 9, 10 and 11 GHz respectively. This result shows that the presented models present a good approximation to the measured data, the proposed present a greater efficiency to the 3GPP model. Therefore, the 3GPP model presents a PLE value equal to 1.73 for a frequency range (0.5 - 100 GHz) and considers only office environment, the proposed presents a range of PLE for the four frequencies studied varying from 1.73 - 2.16 for the corridor and 2.07 - 2.28 for the lab, considering that the environment influences in the mechanisms of propagation and consequently in the received power. Figures 6, 7, 8 and 9 show the curve for the models and

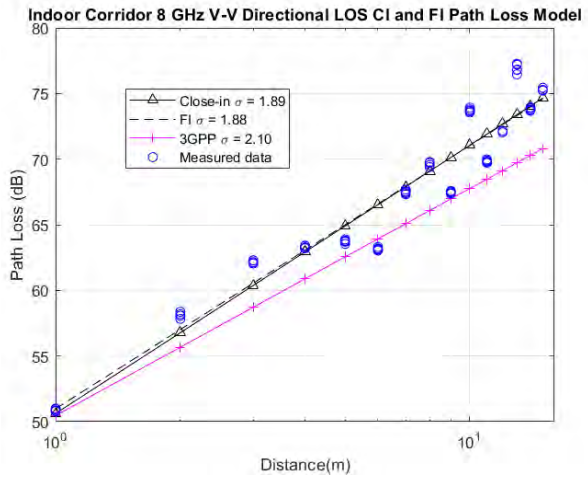

FIGURE 6. 8 Ghz LOS Large-Scale CI, FI And 3GPP Path Loss Model.

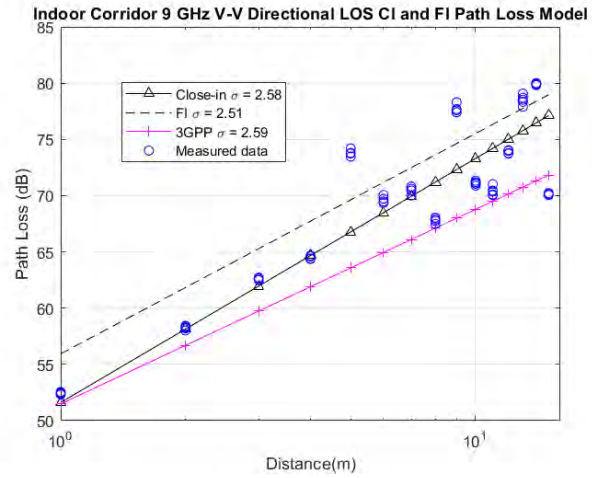

FIGURE 7. 9 Ghz LOS Large-Scale CI, FI And 3GPP Path Loss Model.

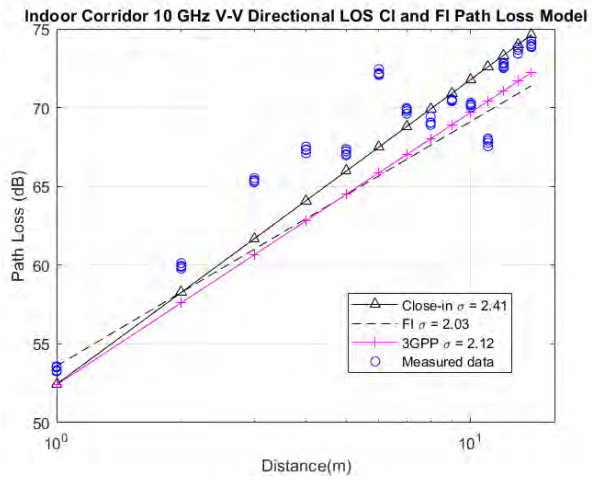

FIGURE 8. 10 Ghz LOS Large-Scale CI, FI And 3GPP Path Loss Model.

data measured along the standard deviation values in the corridor legend. The slope of the curve represented by the PLE, shows to what extent the signal is attenuated with the distance.

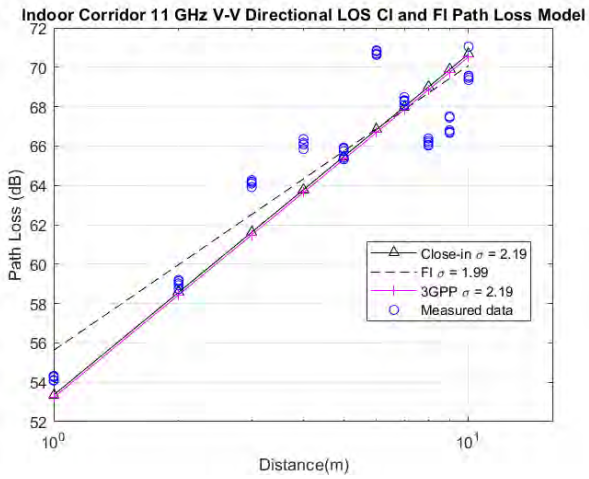

FIGURE 9. 11 Ghz LOS Large-Scale CI, FI And 3GPP Path Loss Model.

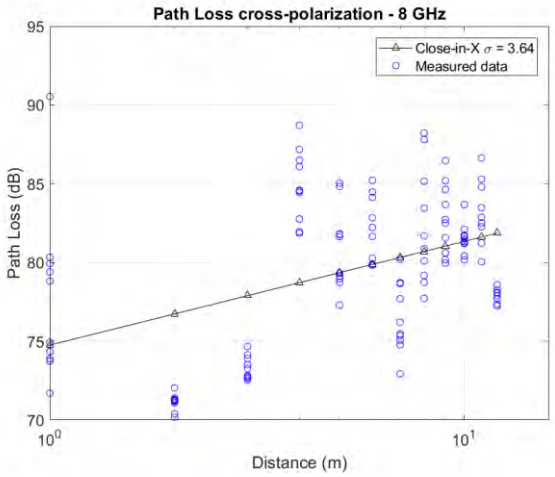

FIGURE 10. 8 GHz directional LOS large-scale CIX path loss model.

As shown in Table 2 and Figures 6, 7, 8 and 9, the PLE has a direct influence on the standard deviation in the average measured data, as well as on how far the signal is attenuated at a distance. Figures 6 and 7 show higher PLE values and standard deviation with regard to Figures 8 and 9. There was a large loss in the signal received for the measurement campaigns that used V-H directional cross-polarized antennas in the corridor. Figs. 10, 11, 12 and 13 illustrate the results of the measured data analysis in the corridor and the close-in-X free space reference model for the frequencies of 8, 9, 10, 11 GHz, in LOS conditions and with V-H directional cross-polarized horn antennas. As shown in Table 2 (as well as the curves in Figs. 10, 11, 12 and 13), the PLE has much lower values with regard to the V-V co-polarization measurements for the same environment. Fig. 11 show a lower initial loss for the average performance of the measured data with regard to Figs. 10, 12 and 13. Figs. 10, 11 and 12, have higher slops compared to CIX to 9 GHz. As a means of understanding the behavioral factors that influence of measurement cross, a small-scale approach is being adopted and/or ray tracing to obtain more details about the multi-paths, as well as the

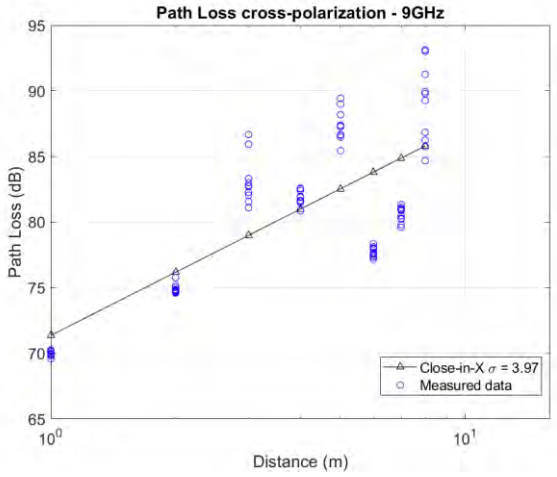

FIGURE 11. 9 GHz directional LOS large-scale CIX path loss model.

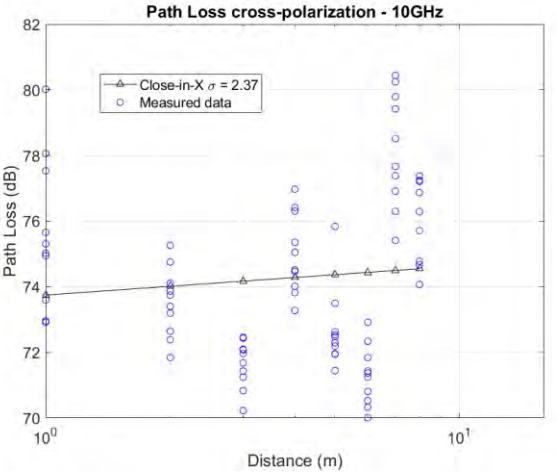

FIGURE 12. 10 GHz directional LOS large-scale CIX path loss model.

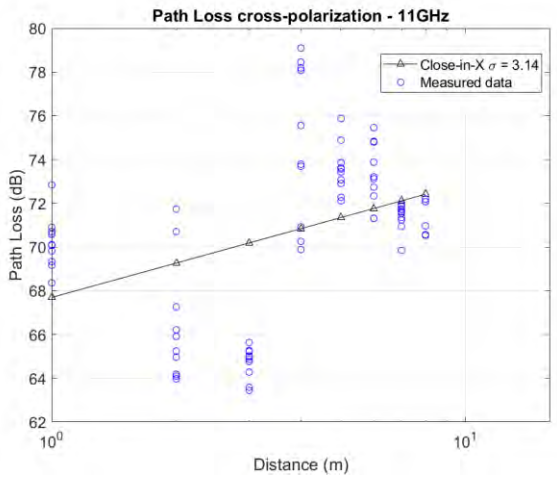

FIGURE 13. 11 GHz directional LOS large-scale CIX path loss model.

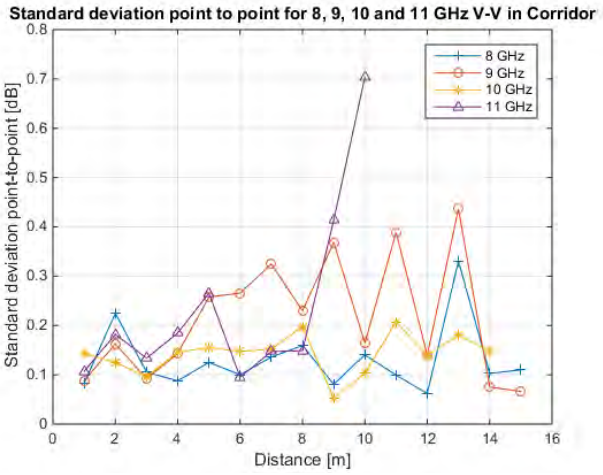

FIGURE 14. Point-to-point standard deviation of data measured in the corridor for frequencies 8, 9, 10 and 11 GHz in the corridor for V-V antennas.

parameters for signal delay and reflections by means of ray tracing techniques.

The results obtained through the measured data found in Table 2 are similar to the parameters of papers in the literature. The article [20] makes large-scale single-frequency and multi-frequency modeling for the 28 GHz and 73 GHz frequency bands within an office. The results for the single-frequency analysis for the PLE parameter were 1.7 and 1.6 for 28 GHz and 73 GHz respectively, analyzing the XPD parameter taking into consideration cross-polarized antennas had 24.7 and 31.4 for 28 GHz and 73 GHz respectively. For ABG and CIF models, in [20] for ABG points out such values for the parameters $\alpha = 0.9$, $\beta = 43.6$ and $\gamma = 1.8$ for the 28 GHz and 73 GHz, for the proposed work parameters calculated were $\alpha = 1.8$ and 2.1 $\beta = 49.11$ and 29.3 $\gamma = 0.47$ and 2.39 for the corridor and laboratory respectively.

The work [19] performs large-scale modeling using CW at frequencies 14 and 22 GHz, for PLE values, referring to Tx height close to the one proposed in this work, resulted in 1.7 and 1.6 14 GHz and 22 GHz.

Analyzing these results obtained in relation to other works we realized that the values of the parameters presented in this work are close to those seen in the literature, even for cases that at a great distance between the frequencies worked, as is the case of 10 GHz to 73 GHz presenting values of PLE very close.

A key approach regarding the measured data is to carry out a statistical survey through the standard deviation. This analysis shows to what extent the signal varies point by point and, on average, for the antenna and cross-polarization discrimination. The point by point standard deviation was calculated for this approach with the aim of determining the signal variation for each meter travelled between the Tx and Rx, for the environments and configuration of the co- and cross-polarization antennas. Fig. 14 shows the LOS point-by-point system in the corridor for the frequencies of 8, 9, 10 and 11 GHz in V-V. It should be noted that there is a low variability in the standard deviation values observed in the Y axis which range from 0 to 0.7 dB. In other words, there is

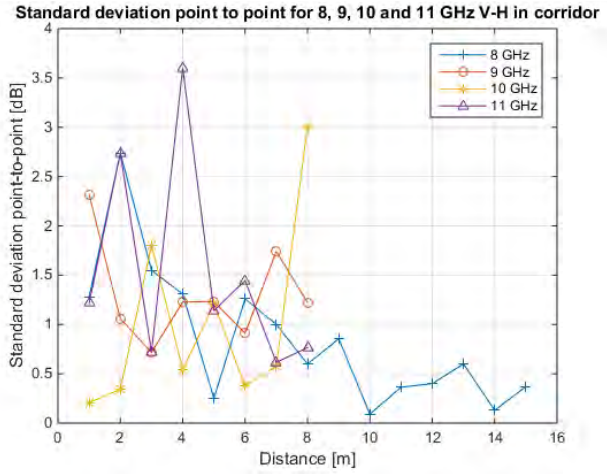

FIGURE 15. Point-to-point standard deviation of data measured in the corridor for frequencies 8, 9, 10 and 11 GHz in the corridor for V-H antennas.

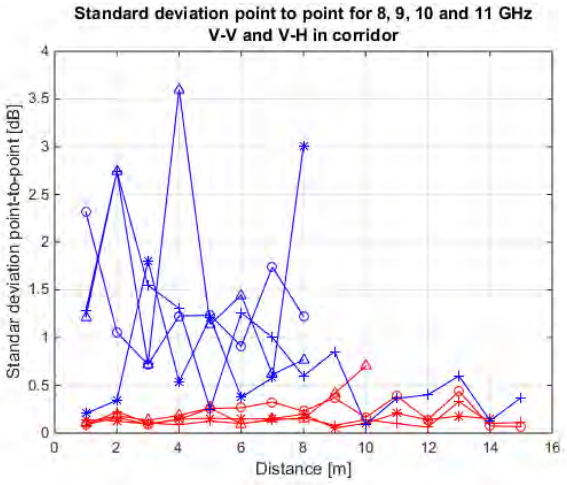

FIGURE 16. Point-to-point standard deviation of data measured in the corridor for frequencies 8, 9, 10 and 11 GHz in the corridor for V-H antennas.

little variation in the power values received for the same point using V-V co-polarization horn antennas in the corridor.

The same system was carried out for V-H cross-polarization antennas with frequencies of 8, 9, 10 and 11 GHz in the corridor. Fig. 15. shows the variations in the standard deviation for each point that was measured (which can be seen in the Y axis), ranging from 0 to 3.5 dB. There is a greater variability of measured data when V-H cross-polarized antennas are used between Tx and Rx. Fig.16 shows the difference in the standard deviation between the co- and cross-polarization, by displaying the point by point standard deviation for the polarizations and the frequencies at the same time.

When the standard deviation in Table 2 and the point-by-point deviation are assessed, it was clear that the standard deviation for the V-V polarization is greater with regard to the V-H. When the point-by-point standard deviation was assessed, it had values lower than those of the V-H (Fig. 16).

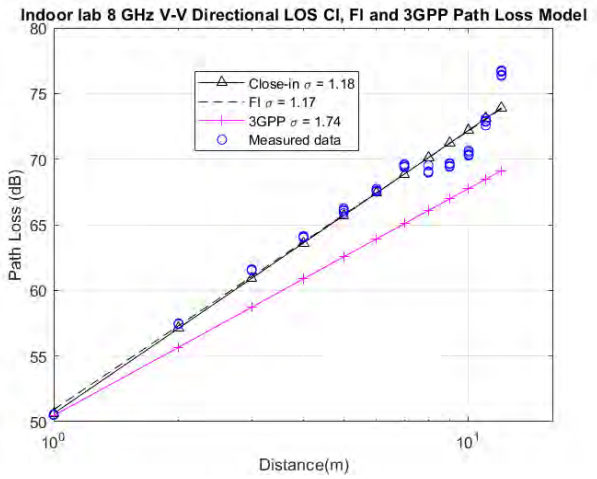

FIGURE 17. 8 Ghz LOS Large-Scale CI, FI And 3GPP Path Loss Model.

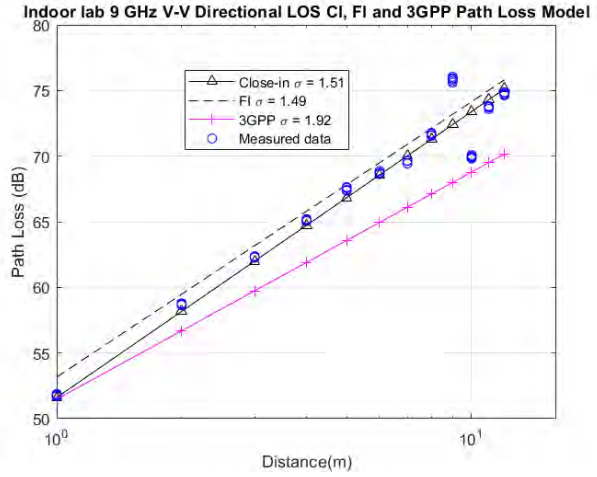

FIGURE 18. 8 Ghz LOS Large-Scale CI, FI And 3GPP Path Loss Model.

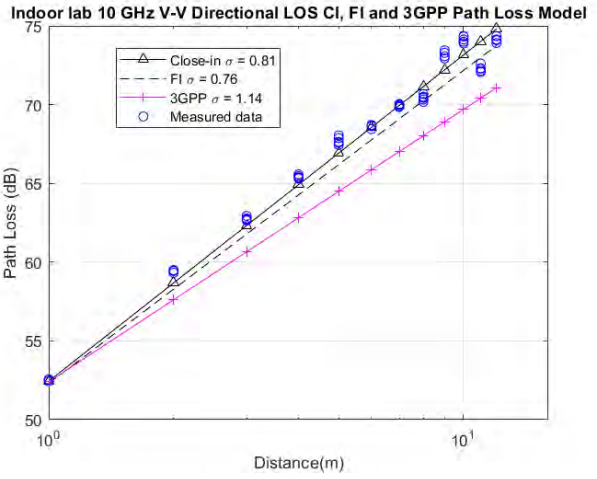

FIGURE 19. 10 Ghz LOS Large-Scale CI, FI And 3GPP Path Loss Model.

B. ANALYSIS IN THE LAB

Figures 17, 18, 19, and 20 show the analysis of the measured data in the laboratory and the performance of the close-in free space reference, FI and 3GPP model for frequencies of 8, 9,

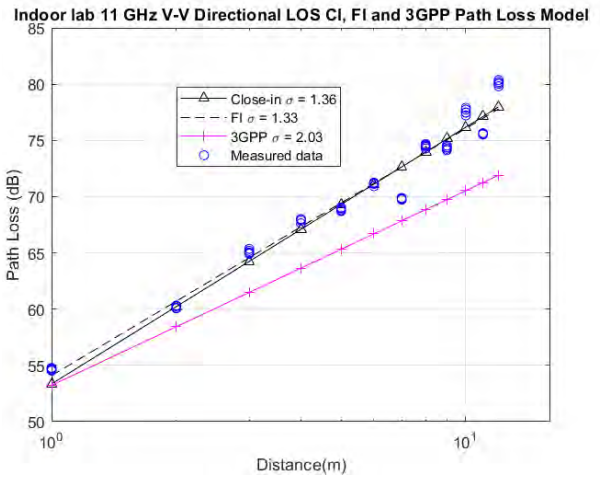

FIGURE 20. 11 Ghz LOS Large-Scale CI, FI And 3GPP Path Loss Model.

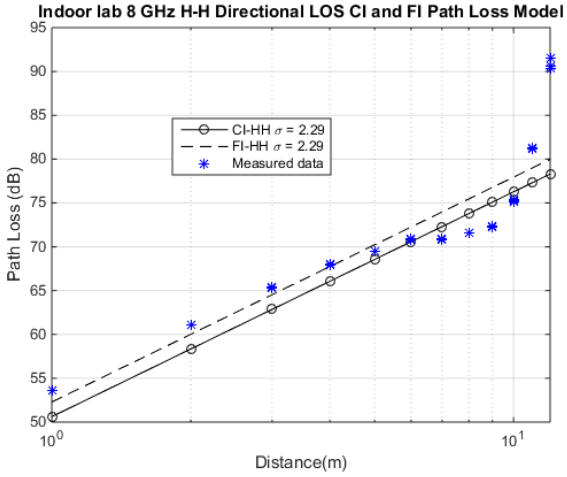

FIGURE 21. 8 GHz LOS large-scale CI-HH path loss model in lab.

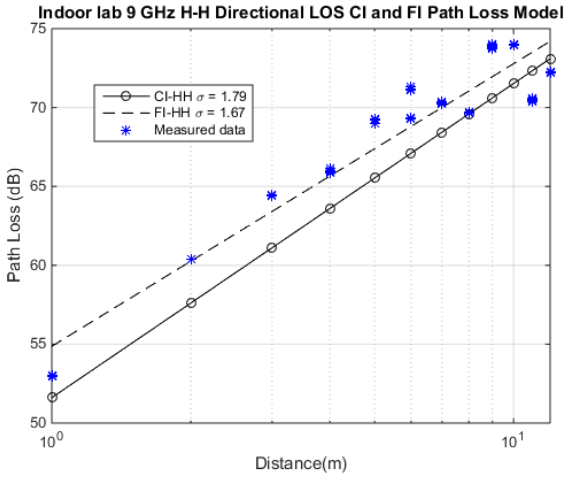

FIGURE 22. 9 GHz LOS large-scale CI-HH path loss model in lab.

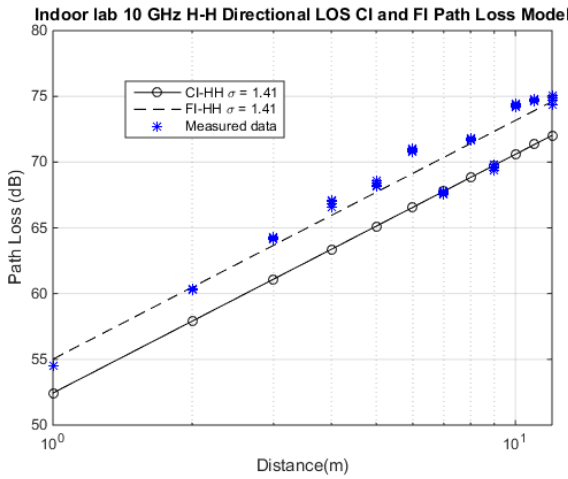

FIGURE 23. 11 GHz LOS large-scale CI-HH path loss model in lab.

10 and 11 GHz in conditions of LOS co-polarization (V-V). In order to compare the accuracy of the proposed models in relation to 3GPP, the standard deviation was calculated in relation to the data measured in the laboratory. For the CI model it obtained: 1.18, 1.51, 0.81 and 1.36; for the FI model the values were: 1.17, 1.49, 0.76 and 1.33; for the 3GPP model the deviation values were: 2.10, 2.59, 2.12 and 2.19 for the frequencies 8, 9, 10 and 11 GHz respectively. In accordance with Table 2, Figures 17, 18, 19 and 20 show the value and slope of the PLE for the close-in model, as well as determining the standard deviation of the measured data. The PLE was radials within the room. The PLE values are different because the closeness of the walls has a direct influence on the signal route and hence on the path loss. When the first radial was defined for the frequency of 10 GHz through the MMSE and for three analyzed, the value of the PLE close to the masonry wall that is formed of bricks, had a greater value for the frequency of 10 GHz. The central radial which was equidistant from the walls, had a PLE value below that of the first radial. Moreover, the third radial close to the wooden wall, had PLE values lower than the first two. This pattern of behavior is caused by the multiple paths that the brick wall causes on account of the reflections; if the wall is wooden the signal passes through it and changes in the middle.

Fig. 21, 22, 23 and 24 show how the measured data behaved and the extension of the CI model for H-H co-polarization. In the case of bands of 8 and 10 GHz, the PLE for H-H values are small than the PLE for the V-V and H-H values, as seen in Table 2. These show higher values of PLE for H-H, and for the frequencies of 9 and 11 GHz and the V-V polarization had higher values for PLE. The performance of the measured data for the frequencies of 8 and 9 GHz for the V-V and H-H antennas are very close and show the feasibility of using either of the two polarized antennas for this environment. In the frequencies of 10 and 11 GHz, the loss values behaved in different ways for the H-H polarization, where there was an increase of approximately 5 dB in the propagation loss with regard to V-V.

The same system is carried out with H-H co-polarization antennas for the frequencies of 8, 9, 10 and 11 GHz in the lab. Fig. 25. shows the variation of the standard deviation for each point that is measured, as seen in the Y axis, which ranges

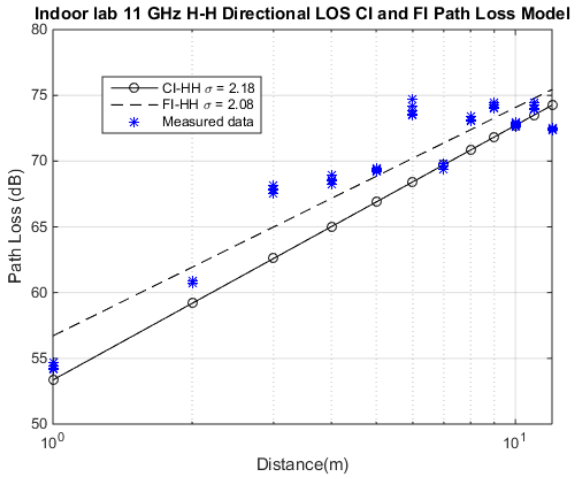

FIGURE 24. 11 GHz LOS large-scale CI-HH path loss model in lab.

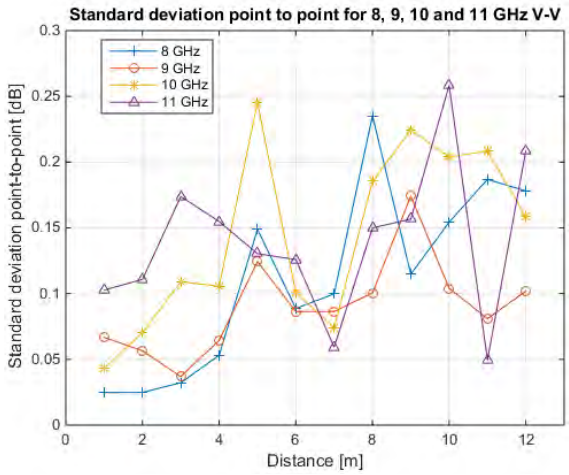

FIGURE 25. Point-to-point standard deviation of data measured in the corridor for frequencies 8 - 11 GHz in the corridor for V-V antennas.

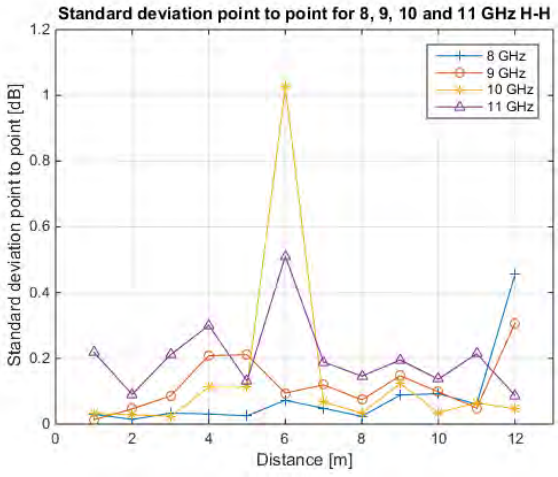

FIGURE 26. Point-to-point standard deviation of data measured in the corridor for frequencies 8 - 11 GHz in the corridor for H-H antennas.

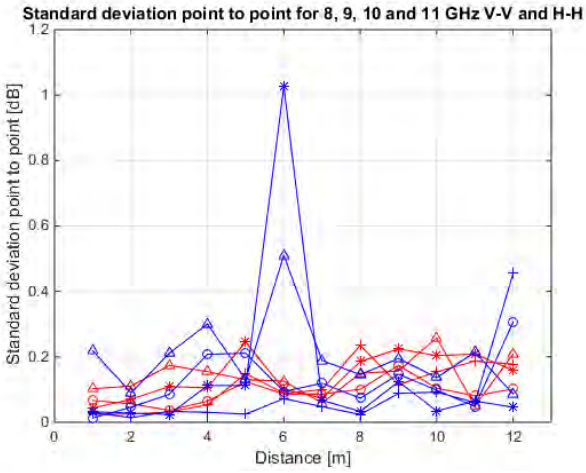

FIGURE 27. P2P standard deviation of data measured in the corridor for V-V and H-H polarization.

from 0 to 1.1 dB; the main fluctuations of the measured data are apparent when H-H cross-polarized antennas are used between the Tx and Rx. A clearer view of the difference of the standard deviation between co-polarization (V-V) and co-polarization (H-H) is seen in Fig. 26, which shows the point-to-point standard deviation by analyzing the polarizations and frequencies at the same time.

C. ANALYSIS SINGLE-FREQUENCY AND MULTI-FREQUENCY

The single: CI and FI and multi-frequency: ABG and CIF models were used to characterize the signal attenuation for frequencies 8, 9, 10 and 11 GHz as a function of frequency and distance for indoor environments.

First, we compared the results for the single analysis for the CI and FI models for the two environments seen in Fig. 28. In Fig. 28(A) and (D) compares $\beta_{FI}/FSPL_{CI}$, and Fig. 28(B) and (E) compares α_{FI}/PLE_{CI} and Fig. 28(C) and (F) compares the standard deviation between the models σ_{FI}/σ_{CI} for the corridor and laboratory respectively. The parameters of the initial loss, $(\beta_{FI}/FSPL_{CI})$ for the corridor and laboratory obtained values above 50 dB and below 54 dB for all the frequencies.

The α_{FI}/PLE_{CI} had values above 1.73 and below 2.28 for all the frequencies and thus it is worth recalling that the values are close to the theoretical PLE = 2. For the standard deviation it was above 0.81 and below 2.59. The variability of the loss parameter with the distance PLE, in Fig. 29 and 30 show above 0.7 and below 1.49. The variability of the loss parameter with the distance PLE, in fig. 29 and 30 present the data measured with the CI models for each frequency with the PLE values, (seen in Table 2), for the corridor and laboratory respectively.

The single parameter variance determined for the CI model demonstrates the slope of the curve for each frequency, and the nature of the PLE analysis for each frequency and environment. This shows that the highest PLE value for the corridor is within the 9 GHz frequency, while for the lab the

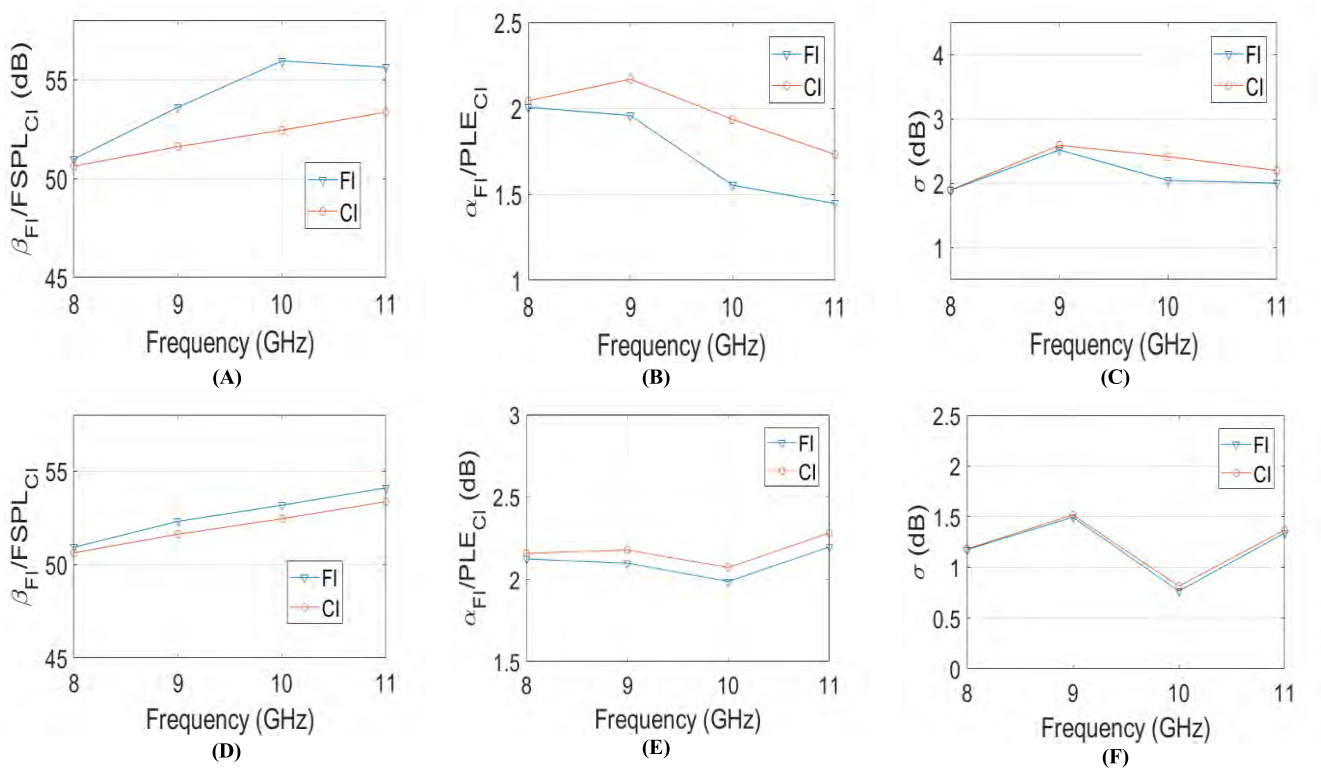

FIGURE 28. Frequency dependence analysis of the single-frequency FI and CI models for frequencies 8, 9, 10 and 11 GHz. (a) and (d) comparing the $\beta_{FI}/FSPL_{CI}$, Fig. 29 (b) and (e) comparing α_{FI}/PLE_{CI} and Fig. 29 (c) and (f) comparing σ_{FI}/σ_{CI} for the corridor and lab respectively.

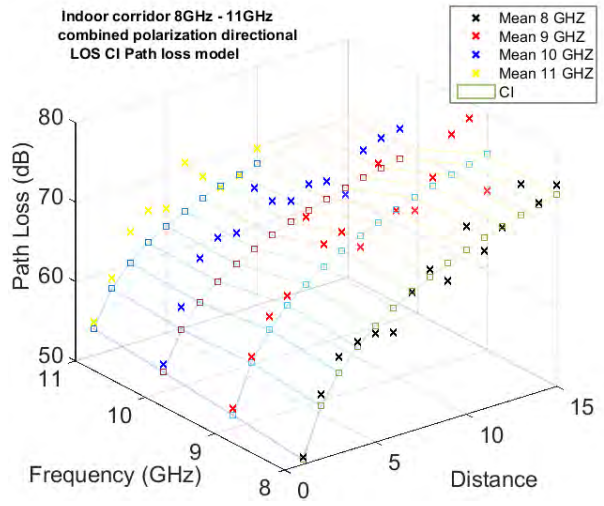

FIGURE 29. PLE Surface plot for frequencies 8 - 11 GHz in the corridor for V-V antennas.

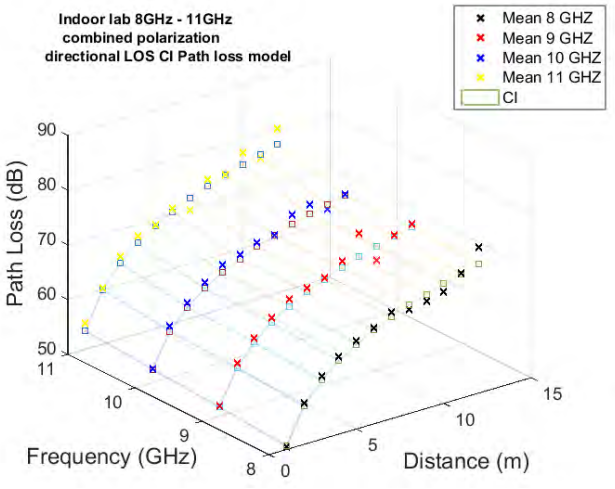

FIGURE 30. PLE Surface plot for frequencies 8 - 11 GHz in the lab for V-V antennas.

highest PLE value is 11 GHz. We compared the results of multi-frequency CIF and ABG path loss models that provide the features of the channel a cross the frequency band. The trajectory loss surface plots and model parameters for CIF and ABG for the two environments are shown in Figs. 31, 32, 33 and 34 and Table 2, respectively. Figs. 33 to 34 and Table 2 show that the CIF and ABG models have very similar parameters for PLE and σ over the entire frequency band. The PLE/α parameters of the CIF and ABG models are within the range of 1.8 above and below 2.18 in all the frequency bands, which agrees well with the theoretical free space PLE of 2, in [20] the author points out such values for the parameters $\alpha = 0.9$, $\beta = 43.6$ and $\gamma = 1.8$ for the 28 GHz and 73 GHz frequencies, these results indicate that since with near frequencies the model parameters values are close what it has been published in the literature. When the frequency dependence factors b with γ, for the CIF are compared, the frequency-dependent parameters are higher in the laboratory measurements (0.1)

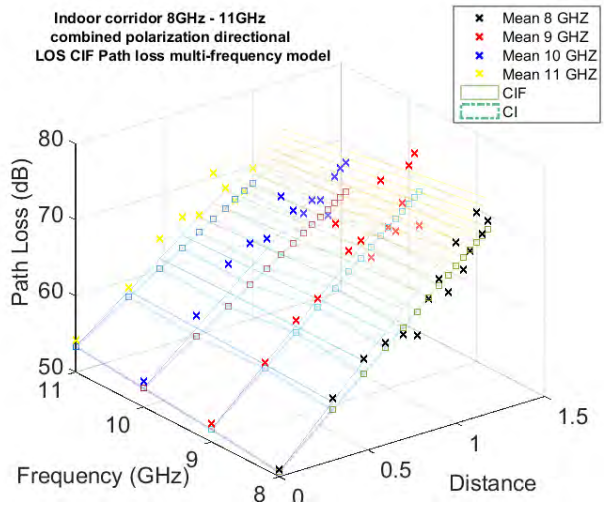

FIGURE 31. Frequency dependence for the CIF model with the CI for the frequencies 8 - 11 GHz in the corridor for V-V antennas.

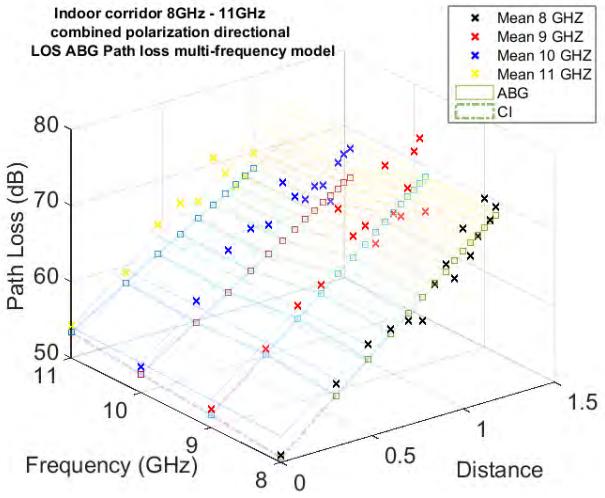

FIGURE 33. Frequency dependency for the ABG model with the CI for frequencies 8 - 11 GHz in the corridor for V-V antennas.

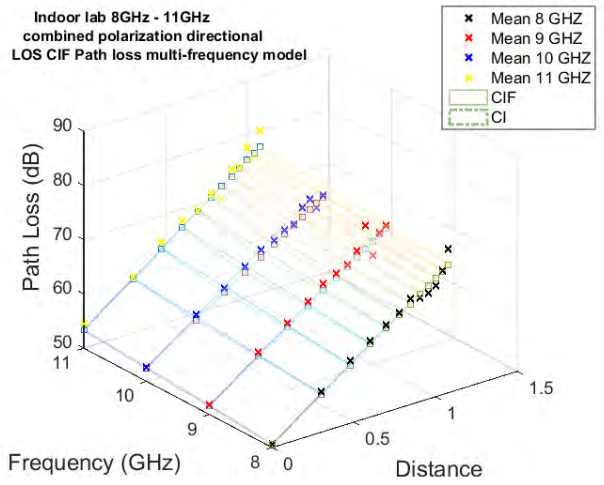

FIGURE 32. Frequency dependence for the CIF model with the CI for the frequencies 8 - 11 GHz in the lab for V-V antennas.

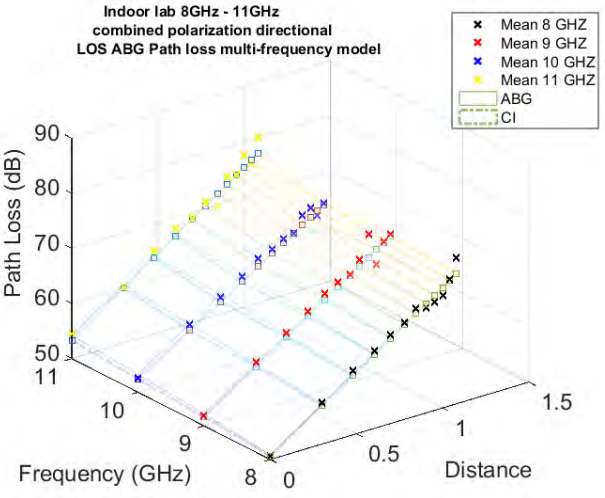

FIGURE 34. Frequency dependency for the ABG model with the CI for frequencies 8 - 11 GHz in the lab for V-V antennas.

than in those in the corridor (-0.35); the parameter f_0 found was 9.35 for the corridor and 9.5 for the laboratory. On the other hand, the γ for the corridor had a value of 0.47 while the laboratory had a value of 2.39. The results show that the CIF has more statistically significant Insights about the frequency dependence on trajectory loss than ABG due to the anchor of path loss based on physics. It was found that the PLE values for the multi-frequency models had a greater stability than the single-frequency, on the other hand the standard deviation for the multi-frequency models was higher than the single-frequency, which led to less precision for the models with multiple frequencies.

D. LOSS CAUSED BY THE WALL

The loss caused by the wall is important because there is a change in the means of propagation between the Tx and Rx, which is directly involved in the intensity and signal path. There are various obstacles (both partial and complete), within indoor environments; this study addresses the question of complete obstruction – that is, it is concerned with the walls or doors.

For OLoS measurement campaigns the transmitter and receiver were 1.5 m above ground with co-polarized antennas (V-V), with elevation and azimuth at 0° to one meter from the obstacle for the Tx and Rx. 10×10001 points were captured for each type of obstacle (masonry, wood and glass).

The measurements for this study include a number of materials such as: wood, bricks, glass and MDF [Medium Density Fireboard]. The frequencies used are the same for LOS conditions, and 8, 9, 10 and 11 GHz with directional horn (V-V) co-polarization antennas. The results for the loss caused by each type of wall and for each band are shown in Table 3.

E. COMPARISON BETWEEN THE MEASURED DATA IN THE CORRIDOR (V-V and V-H) AND LAB (V-V and H-H)

The pattern of the measured data for the two environments shows to what extent the environment influences the propagation loss, as well as the polarization of the antennas. The main parameters of the models used to define a better approximation are as follows: PLE (V-V and H-H), XPD, X_σ and OPLE. The mean standard deviation and point-by-point standard deviation are key factors in analyzing the propagation loss in the whole of its path and each meter travelled, respectively.

It can be determined from an analysis of Table 2 that the PLE values for the corridor are less than those of the lab when V-V co-polarization antennas are employed. This reveals that the attenuation is less intense in the corridor compared with the lab, which can be explained by the features of the corridor and the fact that its shorter length allows more reflections that can be either constructive or destructive. The PLE values remained close for the frequencies of 8, 9 and 10 GHz that use V-V co- polarization guided horn antennas in two environments (Table 2). The PLE values of the corridor are lower than those of the lab for 11 GHz.

The H-H and V-H polarizations differ considerably from each other; the main difference can be seen in the PLE, where H-H has much higher values than V-H. Another difference is the standard deviation since the V-H polarization has lower values than the H-H. However, if the standard deviation is assessed point by point, the H-H polarization has lower values than V-H.

When the V-V polarization is assessed together with the H-H and V-H, it is clear that H-H is the nearest in terms of performance and PLE values, and in some cases the values are very close. V-H proved to be the one that showed the greatest loss, from the nearest point (1 m) to the end of the path, as well as having considerable point-by-point variability since it was the most unstable of the measurements.

The random variable was only analyzed for the CI models, corridor and lab. Fig. 14 and 22 show the signal variation represented by the CI model and random variable (X_σ) together with the measured data and the configurations of the V-V co-polarization antennas. In Fig. 14, it can be noted that the spacing between the frequencies is greater with regard to the fluctuations in Fig. 22. The values in the corridor (Fig. 14) are lower than those in the lab (Fig. 22). This factor is important because it shows the variation of the models with the environments.

V. CONCLUSION

The objective of this study was to examine channel modeling by employing close-in path loss models and their extensions to characterize future wireless channel networks. Close-in models and their extensions have good approximations in LOS and OLOS conditions when directional horn antennas and co- and cross-polarization are used in a corridor and laboratory. The PLE parameter values for the corridor and laboratory (obtained by means of V-V directional antennas), are close to those found in the literature [19] and [20]. However, PLE for V-H cross-polarization antennas have lower values for co-polarization in the same environments.

For modeling purposes, data measured for V-V in LOS situations have higher PLE values than V-H in LOS situations. Since PLE is responsible for the slope of the curve, determining this parameter is paramount for greater accuracy of the modeling in relation to the measured data. For this, the CIX model has a specific PLE in order to reduce the standard deviation between the measured data and the dummy.

Another key analysis that was conducted, concerned mean and point by point standard deviation; in other words, it sought to determine the signal variability per meter travelled as a whole, as well as being linked to the polarizations of the transmitter antennas and receptors. In the case of the corridor, the mean standard deviation and the values of the standard deviation for frequencies of 8 and 9 GHz, have greater values than those with 10 and 11 GHz. With regard to point-by-point standard deviation, it was confirmed that the use of V-V co-polarization antennas, resulted in little variation and remained between 0 to 0.7 dB, (as seen in Fig. 15). In the case of V-H cross-polarized antennas, there was greater variability in the standard deviation, which went from 0 to 3.5 dB (Fig. 16).

When the measurements were carried out in the laboratory with V-V and H-H directional antennas (by means of close-in models and extensions), they showed different PLE values for each frequency and polarization, particularly for frequencies of 8 GHz and 10 GHz. The PLE values for H-H antennas are higher than those of the V-V, for frequencies of 9 GHz and 11 GHz, while the PLE value was higher for the V-V than the H-H.

The influence of the walls is different for each of the obstacles and the propagation loss changes in accordance with the frequency - the greater the frequency, the greater the loss experienced. The study of propagation loss for the total OLOS (complete obstruction) is a key factor, because the shorter the wavelength, the greater the propagation loss will be, when obstacles are encountered. Future telecommunications systems should be able to circumvent this problem because millimeter waves will be used.

Another point is the need to distinguish between the waves that are propagated within different environments, however they might be confined. The reflections are more intense in the corridor owing to the proximity of the walls, as well as the kind of material used in constructing the walls, floor and ceiling, together with the metal grilles and panels. The laboratory is a more extensive environment and is formed in a different way from the corridor. It has walls built of brick and wood, as well as being furnished with chairs, tables and desktops. These features affect the path loss of the electromagnetic waves of these environments and in this study, showed their differences through close-in free space path loss models, together with their extensions and standard deviation.

In future studies, a small-scale approach will be adopted for the frequencies used here of 8, 9, 10 and

11 GHz, measurements. This will be accompanied by a large-scale approach in higher frequencies of 28 GHz to 93 GHz for indoor environments, and the modeling of path loss by means of directional and omni antennas.

REFERENCES

[1] A. M. Al-Samman *et al.*, "Statistical modelling and characterization of experimental mm-wave indoor channels for future 5G wireless communication networks," *PLoS ONE*, vol. 11, no. 9, Sep. 2016, Art. no. e0163034.

[2] S. Chitra and N. Kumaratharan, "Intercarrier interference reduction in MC-CDMA system through second order duobinary coded phase rotated conjugate cancellation scheme," *PLoS ONE*, vol. 10, no. 3, Mar. 2015, Art. no. e0116326.

[3] M. N. Hindia, A. W. Reza, K. A. Noordin, and M. H. R. Chayon, "A novel LTE scheduling algorithm for green technology in smartGrid," *PLoS ONE*, vol. 10, no. 4, Apr. 2015, Art. no. e0121901.

[4] T. S. Rappaport *et al.*, "Millimeter wave mobile communications for 5G cellular: It will work!" *IEEE Access*, vol. 1, pp. 335–349, 2013. doi: 10.1109/ACCESS.2013.2260813.

[5] Z. Pi and F. Khan, "An introduction to millimeter-wave mobile broadband systems," *IEEE Commun. Mag.*, vol. 49, no. 6, pp. 101–107, Jun. 2011. doi: 10.1109/MCOM.2011.5783993.

[6] T. S. Rappaport, G. R. MacCartney, M. K. Samimi, and S. Sun, "Wideband millimeter-wave propagation measurements and channel models for future wireless communication system design," *IEEE Trans. Commun.*, vol. 63, no. 9, pp. 3029–3056, Sep. 2015. doi: 10.1109/TCOMM.2015.2434384.

[7] *METIS Deliverable D1.4. METIS Channel Models*, Feb. 2015.

[8] *Channel Modeling for Higher Frequency Bands*. document RP151306, 3GPP, Jun. 2015.

[9] *5G Millimeter Wave Channel Model Alliance*. Accessed: Nov. 5, 2017. [Online]. Available: http://www.nist.gov/ctl/upload/5G-Millimeter-Wave-Channel-Model-AllianceV2.pdf

[10] *METIS Deliverable D1.4, Proposed Solutions for New Radio Access*, Feb. 2015.

[11] H. K. Rath, S. Timmadasari, B. Panigrahi, and A. Simha, "Realistic indoor path loss modeling for regular WiFi operations in India," in *Proc. 23rd Nat. Conf. Commun. (NCC)*, vol. 1, Mar. 2017, pp. 1–6.

[12] M. F. Iskander and Z. Yun, "Propagation prediction models for wireless communication systems," *IEEE Trans. Microw. Techn.*, vol. 50, no. 3, pp. 662–673, Mar. 2002. doi: 10.1109/22.989951.

[13] Y. Okumura, E. Ohmori, T. Kawano, and K. Fukuda, "Field strength and its variability in VHF and UHF land-mobile radio service," *Rev. Electr. Commun. Lab.*, vol. 16, no. 9, pp. 825–873, 1968.

[14] E. Damosso and L. M. Correia, *COST Action 231: Digital Mobile Radio Towards Future Generation Systems: Final Report*. Brussels, Belgium: European Commission, 1999.

[15] C. Phillips, D. Sicker, and D. Grunwald, "A survey of wireless path loss prediction and coverage mapping methods," *IEEE Commun. Surveys Tuts.*, vol. 15, no. 1, pp. 255–270, 1st Quart., 2013.

[16] K. Haneda, "Channel models and beamforming at millimeter wave frequency bands," *IEICE Trans. Commun.*, vol. 98, no. 5, pp. 755–772, May 2015.

[17] A. F. Molisch *et al.*, "Millimeter-wave channels in urban environments," presented at the 10th Eur. Conf. Antennas Propag. (EuCAP), Davos, Switzerland, Apr. 2016.

[18] X. Zhou, *et al.* "Indoor wideband channel measurements and analysis at 11 and 14 GHz," *IET Microw., Antennas Propag.*, vol. 11, no. 10, pp. 1393–1400, Aug. 2017.

[19] N. O. Oyie and T. J. O. Afullo, "Measurements and analysis of large-scale path loss model at 14 and 22 GHz in indoor corridor," *IEEE Access*, vol. 6, pp. 17205–17214. doi: 10.1109/ACCESS.2018.2802038.

[20] G. R. MacCartney, T. S. Rappaport, S. Sun, and S. Deng, "Indoor office wideband millimeter-wave propagation measurements and channel models at 28 and 73 GHz for ultra-dense 5G wireless networks," *IEEE Access*, vol. 3, pp. 2388–2424, 2015. doi: 10.1109/ACCESS.2015.2486778.

[21] A. Hrovat, G. Kandus, and T. Javornik, "Path loss analyses intunnels and underground corridors," *Int. J. comm*, vol. 6, no. 3, pp. 136–144, Aug. 2012.

[22] V. S. Abhayawardhana, I. J. Wassell, D. Crosby, M. P. Sellars, and M. G. Brown, "Comparison of empirical propagation path loss models for fixed wireless access systems," in *Proc. IEEE 61st Veh. Technol. Conf.*, May/Jun. 2005, pp. 73–77.

[23] K. Aki *et al.*, "Path loss models with distance-dependent weighted fitting and estimation of censored path loss data," *IET Microw., Antennas Propag.*, vol. 10, no. 14, pp. 1467–1474, Nov. 2016.

[24] S. Hur *et al.*, "Wideband spatial channel model in an urban cellular environments at 28 GHz," in *Proc. 9th Eur. 9th Eur. Conf. Antennas Propag. (EuCAP)*, Lisbon, Portugal, Apr. 2015, pp. 1–5.

[25] T. S. Rappaport, *Wireless Communications: Principles and Practice*, 2nd ed. Upper Saddle River, NJ, USA: Prentice-Hall, 2002.

[26] T. S. Rappaport and D. A. Hawbaker, "Effects of circular and linear polarized antennas on wideband propagation parameters in indoor radio channels," in *Proc. IEEE Global Telecommun. Conf. GLOBECOM*, vol. 2, Dec. 1991, pp. 1287–1291.

[27] C. M. P. Ho, T. S. Rappaport, and M. P. Koushik, "Antenna effects on indoor obstructed wireless channels and a deterministic image-based wide-band propagation model for in-building personal communication systems," *Int. J. Wireless Inf. Netw.*, vol. 1, no. 1, pp. 61–76, Jan. 1994.

[28] T. S. Rappaport, *Wireless Communications: Principles and Practice*, 2nd ed. Upper Saddle River, NJ, USA: Prentice-Hall, 2002.

[29] T. S. Rappaport and D. A. Hawbaker, "Wide-band microwave propagation parameters using circular and linear polarized antennas for indoor wireless channels," *IEEE Trans. Commun.*, vol. 40, no. 2, pp. 240–245, Feb. 1992.

[30] J. Zhu, H. Wang, and W. Hong, "Large-scale fading characteristics of indoor channel at 45-GHz band," *IEEE Antennas Wireless Propag. Lett.*, vol. 14, pp. 735–738, 2015.

[31] R. R. Skidmore, T. S. Rappaport, and A. L. Abbott, "Interactive coverage region and system design simulation for wireless communication systems in multioored indoor environments: SMT Plus," in *Proc. 5th IEEE Int. Conf. Universal Pers. Commun.*, vol. 2, Sep. 1996, pp. 646–650.

[32] A. G. M. Lima and L. F. Menezes, "Motley-Keenan model adjusted to the thickness of the wall," in *IEEE MTT-S Int. Microw. Symp. Dig.*, Jul. 2005, pp. 180–182. doi: 10.1109/IMOC.2005.1580040.

[33] F. J. B. Barros, R. D. Vieira, and G. L. Siqueira, "Relationship between delay spread and coherence bandwidth for UWB transmission," in *IEEE MTT-S Int. Microw. Symp. Dig.*, Jul. 2005, pp. 415–420. doi: 10.1109/IMOC.2005.1580033.

[34] F. J. B. Barros, E. Costa, G. L. Siqueira, and J. R. Bergmann, "A site-specific beam tracing model of the UWB indoor radio propagation channel," *IEEE Trans. Antennas Propag.*, vol. 63, no. 8, pp. 3681–3694, Aug. 2015. doi: 10.1109/TAP.2015.2440475.

[35] F. J. B. Barros *et al.*, "Channel model and data analysis for indoor environment," in *Proc. 6th Eur. Conf. Antennas Propag. (EUCAP)*, Prague, Czech Republic, Mar. 2012, pp. 2051–2054. doi: 10.1109/EuCAP.2012.6206241.

[36] J. W. McKown and R. L. Hamilton, "Ray tracing as a design tool for radio networks," *IEEE Netw.*, vol. 5, no. 6, p. 27–30, Nov. 1991.

[37] G. E. Athanasiadou, A. R. Nix, and J. P. McGeehan, "A ray tracing algorithm for microcellular wideband propagation modelling," in *Proc. IEEE 45th Veh. Technol. Conf.*, vol. 1, Jul. 1995, pp. 261–265.

[38] K. R. Schaubach, N. J. Davis, and T. S. Rappaport, "A ray tracing method for predicting path loss and delay spread in microcellular environments," in *Proc. Veh. Technol. Soc. 42nd VTS Conf.-Frontiers Technol.*, May. 1992, pp. 932–935.

[39] S. Deng, G. R. MacCartney, and T. S. Rappaport "Indoor and outdoor 5g diffraction measurements and models at 10, 20, and 26 GHz," in *Proc. IEEE Global Commun. Conf. (GLOBECOM)*, Dec. 2016, pp. 1–7.

[40] J. Ryan, G. R. MacCartney, and T. S. Rappaport, "Indoor office wideband penetration loss measurements at 73 GHz," in *Proc. IEEE Int. Conf. Commun. Workshops (ICC Workshops)*, Paris, France, May 2017, pp. 228–233. doi: 10.1109/ICCW.2017.7962662.

[41] D. Metis, *Intermediate Description of the Spectrum Needs and Usage PrinciplesV1.0*, document ICT-317669, METIS project, Aug. 2013.

[42] C. Wang, J. Bian, J. Sun, W. Zhang, and M. Zhang, "A Survey of 5G Channel Measurements and Models," *IEEE Commun. Surveys Tuts.* doi: 10.1109/COMST.2018.2862141.

[43] A. M. Al-samman, T. A. Rahman, and M. H. Azmi, "Indoor corridor wideband radio propagation measurements and channel models for 5G millimeter wave wireless communications at 19 GHz, 28 GHz, and 38 GHz bands," *Wireless Commun. Mobile Comput.* vol. 2018, Jan. 2018, Art. no. 6369517. doi: 10.1155/2018/6369517.

[44] A. M. Al-samman, T. A. A. Rahman, M. H. Azmi, and S. A. Al-Gailani, "Millimeter-wave propagation measurements and models at 28 GHz and 38 GHz in a dining room for 5G wireless networks," *Measurement*, vol. 130, pp. 71–81, Dec. 2018. doi: 10.1016/j.measurement.2018.07.073.

[45] M. Kim, Y. Konishi, Y. Chang, and J.-I. Takada, "Large Scale Parameters and Double-Directional Characterization of Indoor Wideband Radio Multipath Channels at 11 GHz," *IEEE Trans. Antennas Propag.*, vol. 62, no. 1, pp. 430–441, Jan. 2014. doi: 10.1109/TAP.2013.2288633.
[46] *Due to Procedural Differences at FCC and Ofcom there is more Redundancy in the Documents Filed at FCC than those at Ofcom.* [Online]. Available: http://apps.fcc.gov/ecfs/proceeding/view/view?name=14-177

IURY DA SILVA BATALHA was born in Belém, Pará, Brazil, in 1991. He received the M.Sc. degree in electronic engineering from the Federal University of Pará, in 2016, where he is currently pursuing the Ph.D. degree.

His current research interests include electrical engineering and computing, especially in telecommunications and applied computing, particularly in mobile networks, propagation, and electromagnetic compatibility.

ANDRÉA V. R. LOPES was born in Belém, Pará, Brazil, in 1991. She received the Degree in computer engineering from the Federal University of Pará, with training, in 2018. Her current research interests include propagation, antennas, indoor empirical models, 5G technology, and channel modeling.

JASMINE P. L. ARAÚJO (M'87) received the B.Sc., master's, and D.Sc. degree in electrical engineering from the Federal University of Pará, in 1994, 2002, and 2011, respectively, and the Ph.D. degree from INESC-TEC, Porto, in 2015. She is currently an Adjunct Professor with the Federal University of Pará. Her current research interests include electrical engineering, especially in telecommunications and applied computing, and particularly mobile networks, propagation, electromagnetic compatibility, and bio-inspired algorithms.

BRUNO L. S. CASTRO was born in Belém, Pará, Brazil, in 1984. He received the Degree in telecommunications engineering from the Amazon Superior Studies Institute (IESAM), and the master's and D.Sc. degrees in electrical engineering from the Federal University of Pará, in 2010 and 2014, respectively.

His current research interests include electrical engineering, especially in telecommunications, particularly in signal propagation, wireless communications, and the Internet of Things.

FABRÍCIO J. B. BARROS received the B.Sc. degree from the Federal University of Pará, Belém, Brazil, in 2003, and the M.Sc. and Ph.D. degrees from the Pontifical Catholic University of Rio de Janeiro, Brazil, in 2005 and 2010, respectively, all in electrical engineering.

He has been an Adjunct Professor with the Federal University of Pará, Brazil, since 2012. His research interests include the modeling and analysis of antennas, experimental activities, and simulations based on the finite difference time domain method, and beam tracing methods to characterize radio propagation channels.

GERVÁSIO PROTÁSIO DOS SANTOS CAVALCANTE (M'74) received the M.S. degree in electronic engineering from Federal University of Paraíba, Campina Grande, Brazil, and the Ph.D. degree in telecommunications engineering with UNICAMP—Estate University of Campinas, Brazil, in 1982.

From 1974 to 2000, he was a Titular Professor with the Electrical Engineering Department, and since 2001, he has been a Titular Professor with the Computation and Telecommunication Faculty, Federal University of Pará, Brazil. His research interests include the development of models for wire antennas in communications, and the frequency selective surface theory using bio-inspired multi-objective algorithms.

EVALDO GONÇALVES PELAES received the Degree in electrical engineering and the Full Degree in physics from the Federal University of Pará, in 1977, the master's degree in electrical engineering from the Pontifical Catholic University of Rio de Janeiro, in 1982, and the Ph.D. degree in electrical engineering from the State University of Campinas, in 1998. He is currently an Associate Professor with the Federal University of Pará. He has experience in electrical engineering, with an emphasis on signal processing, and mainly works in signal processing, wavelet transform, image coding, propagation models, mobile communications, and quality power.